Detection and Spectral Analysis of Trifluoromethyl Groups at a Surface by Sum Frequency Generation Vibrational Spectroscopy

Mark A. Even, Sang-Ho Lee, Jie Wang, and Zhan Chen*

Department of Chemistry, 930 North University Avenue, University of Michigan, Ann Arbor, Michigan 48109

Received: August 12, 2006; In Final Form: October 6, 2006

Sum frequency generation (SFG) vibrational spectroscopy was used to detect the presence of trifluoromethyl groups on the surface of 4-(trifluoromethyl)benzyl alcohol (TFMBA) in air. Supplementary data from infrared and Raman spectra were correlated to ab initio calculations by use of density functional theory (DFT) for TFMBA and three related compounds to reliably assign vibrational modes to the spectra. It was shown that strongly ordered CF_3 groups dominate the surface of the TFMBA, and the vibrational modes of this functional group are strongly coupled to the benzene ring of the benzyl alcohol. This coupling, along with the SFG activity of the CF_3 group, is removed with the insertion of an oxygen atom between the CF_3 group and the benzene ring.

1. Introduction

The surfaces of fluorocarbons have long been of interest because of their unique properties.[1] Fluorine is very small and electronegative, so the C−F bond is very strong and ionic in character and exhibits very low polarizability. Perfluorocarbons therefore exhibit very weak intermolecular interactions, resulting in materials with low surface energies or "inert surfaces". Fluorinated polymers in particular have found use as water-repellent or chemically resistant films. Recently, coatings have been developed with the intention of using the low surface energy of perfluorocarbons to improve the fouling release properties of marine antifouling films.[2−5] The surface properties of these materials depend on the ordering and surface coverage of the perfluorocarbon structures.[6−13]

Many different techniques have been applied to characterize surface structure and composition. Contact angle goniometry, X-ray photoelectron spectroscopy, secondary ion mass spectrometry, near-edge X-ray absorption fine structure spectroscopy, ellipsometry, neutron reflectivity, and infrared (IR) and Raman spectroscopy have all been used to study surfaces, and excellent results have been generated from such studies. However, many of these techniques require a high vacuum environment or lack the surface selectivity needed to determine information about functional group coverage and orientation at surfaces with monolayer sensitivity.[14,15] Recently, sum frequency generation (SFG) vibrational spectroscopy has been developed into a powerful tool to study various surfaces in situ in a variety of environments.[16−32] SFG is a nonlinear optical vibrational spectroscopy that has submonolayer surface sensitivity. More details regarding SFG theory and technology will be presented below.

SFG has already been successfully applied to detect signals from CF_2 groups.[33] However, up to now the detection of SFG signals from CF_3 groups has not been reported, although the ordering and orientation of interfacial CF_3 groups have been studied by other techniques.[34] In this research, we detected SFG signals from CF_3 groups from a fluorinated liquid compound, 4-(trifluoromethyl)benzyl alcohol (TFMBA). To reliably analyze SFG signals, infrared and Raman spectroscopy have been applied to study TFMBA and several derivatives, 4-methylbenzyl alcohol (MBA), 4-(trifluoromethoxy)benzyl alcohol (TFMOBA), and 4-methoxybenzyl alcohol (MOBA), to determine where vibrational modes of the CF_3 group can be found. The molecular formulas for these four compounds are shown in Chart 1. Ab inito calculations using density functional theory (DFT) were utilized to analyze and interpret IR and Raman vibrational spectra of these compounds. Such analysis has been correlated to SFG studies, which verifies the detection of ordered CF_3 groups in TFMBA by SFG.

CHART 1: Molecular Formulas for TFMBA, TFMOBA, MBA, and MOBA

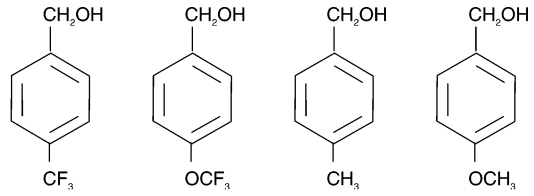

TFMBA TFMOBA MBA MOBA

2. Experimental Section

2.1. Samples. Liquid TFMBA (98%), TFMOBA (97%), MOBA (98%), and solid MBA (98%) were purchased from Aldrich and used as received.

2.2. Sum Frequency Generation Spectroscopy. SFG is a process in which two input beams at frequencies ω_1 and ω_2 mix in a medium and generate an output beam at the sum frequency $\omega = \omega_1 + \omega_2$.[16−32] Usually ω_1 is in the visible range, and ω_2 is a tunable infrared beam. If ω_2 is scanned over the vibrational resonances of molecules, the SFG is resonantly enhanced, producing a vibrational spectrum characteristic of the material. As a second-order nonlinear optical process, SFG spectral intensity will be zero in a medium with inversion symmetry under the electric-dipole approximation. SFG spectra can be detected from a material where the inversion symmetry

* To whom correspondence should be addressed: e-mail zhanc@umich.edu; fax 734-647-4865.

10.1021/jp065221r CCC: $33.50
Published on Web 11/29/2006

TABLE 1: Definitions of Local Symmetry Coordinates[a]

local symmetry coordinates S	TFMBA/MBA	TFMOBA/MOBA
sCO	s23	s23
asCH_2	s34 − s35	s34 − s35
ssCH_2	s34 + s35	s34 + s35
abOCH	b234 − b235	b234 − b235
sbOCH	b234 + b235	b234 + b235
atCH_2	t1-4 − t1-5	t1-4 − t1-5
stCH_2	t1-4 + t1-5	t1-4 + t1-5
as1CF_3/as1CH_3	2s1617 − s1618 − s1619	−s1718 − s1719 + 2s1720
as2CF_3/as2CH_3	−s1618 + s1619	−s1718 + s1719
ssCF_3/ssCH_3	s1617 + s1618 + s1619	s1718 + s1719 + s1720
ab1CF_3/ab1CH_3	2b111617 − b111618 − b111619	−b161718 − b161719 + 2b161720
ab2CF_3/ab2CH_3	−b111618 + b111619	−b161718 + b161719
sbCF_3/sbCH_3	b111617 + b111618 + b111619	b161718 + b161719 + b161720
at1CF_3/at1CH_3	2t9-17 − t9-18 − t9-19	−t11-18 − t11-19 + 2t11-20
at2CF_3/at2CH_3	−t9-18 + t9-19	−t11-18 + t11-19
stCF_3/stCH_3	t9-17 + t9-18 + t9-19	t11-18 + t11-19 + t11-20

[a] Abbreviations: s = stretching, b = bending, t = torsion, as = asymmetric stretching, ss = symmetric stretching, ab = asymmetric bending, sb = symmetric bending, at = asymmetric torsion, and st = symmetric torsion. Each symmetry coordinate is normalized to unity in our calculations. Such abbreviations have also been used in Tables 2−5.

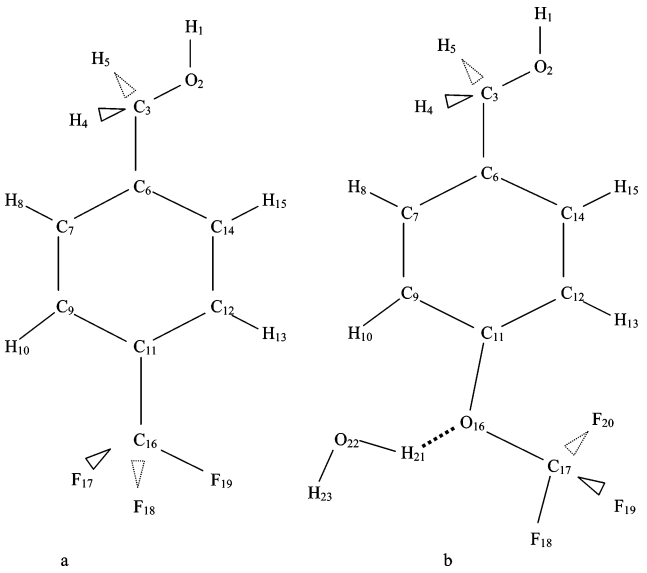

Figure 1. Ab initio optimized geometry for (a) TFMBA and (b) TFMOBA.

is broken. Most bulk materials have inversion symmetry and do not generate SFG signals. At surfaces or interfaces, where inversion symmetry is necessarily broken, SFG is allowed and can therefore be used as an effective surface/interface probe. Both experimental results and theoretical calculations indicate that SFG is submonolayer-sensitive for simple surfaces and interfaces.

Two custom-designed SFG setups in our lab are composed of four components each: a picosecond Nd:YAG laser, a harmonic unit with two KD*P crystals, an optical parametric generation (OPG)/optical parametric amplification (OPA) and difference frequency generation (DFG) system based on LBO and $AgGaS_2$ (or GaSe) crystals, and a detection system. The visible beam (532 nm) is generated by frequency-doubling the fundamental output pulses of 20 ps pulse width from the Nd:YAG laser. The IR beam can be tuned from 650 to 4300 cm^{-1}, generated from the OPG/OPA/DFG system. The incident angles of the visible and IR input beams can be varied. In a standard experiment, they are 60° and 55° versus the surface normal, respectively. The diameters of both visible and IR beams at the surface are about 500 μm. The SFG signal from the surface is collected by a photomultiplier and processed with a gated integrator. SFG spectra can be normalized by the power of the

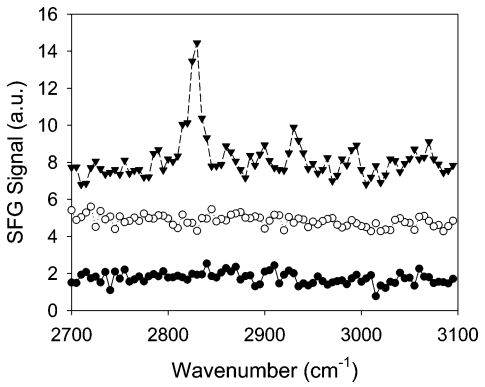

Figure 2. SFG spectra collected from MOBA (top), TFMBA (middle), and TFMOBA (bottom) in air in the C−H stretching region by use of the ssp polarization combination.

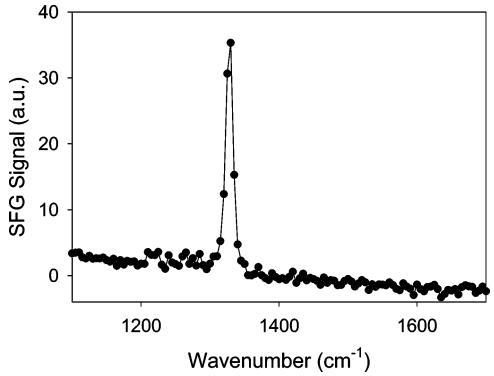

Figure 3. SFG spectrum (ssp) collected from TFMBA in air.

input laser beams. In this project, only SFG spectra with the ssp polarization combination were collected; we were unable to detect SFG spectra with the sps polarization combination.

2.3. Raman Spectroscopy. Raman spectra were obtained by use of a Renishaw inVia Raman microscope equipped with a 633 nm HeNe laser and a 1200 lines/mm grating. Spectra were collected with an Olympus SLMPlan 20× objective (numerical aperture = 0.35) and 50 μm slit in extended scan mode with a range of 500−3400 cm^{-1} and adding five scans. The liquid samples were placed in a quartz cuvette for analysis, and the solid sample was placed on low-background aluminum foil. Spectra were collected and analyzed with the WiRE 2.0 software package. Calibration was performed by use of neon and silicon standards.

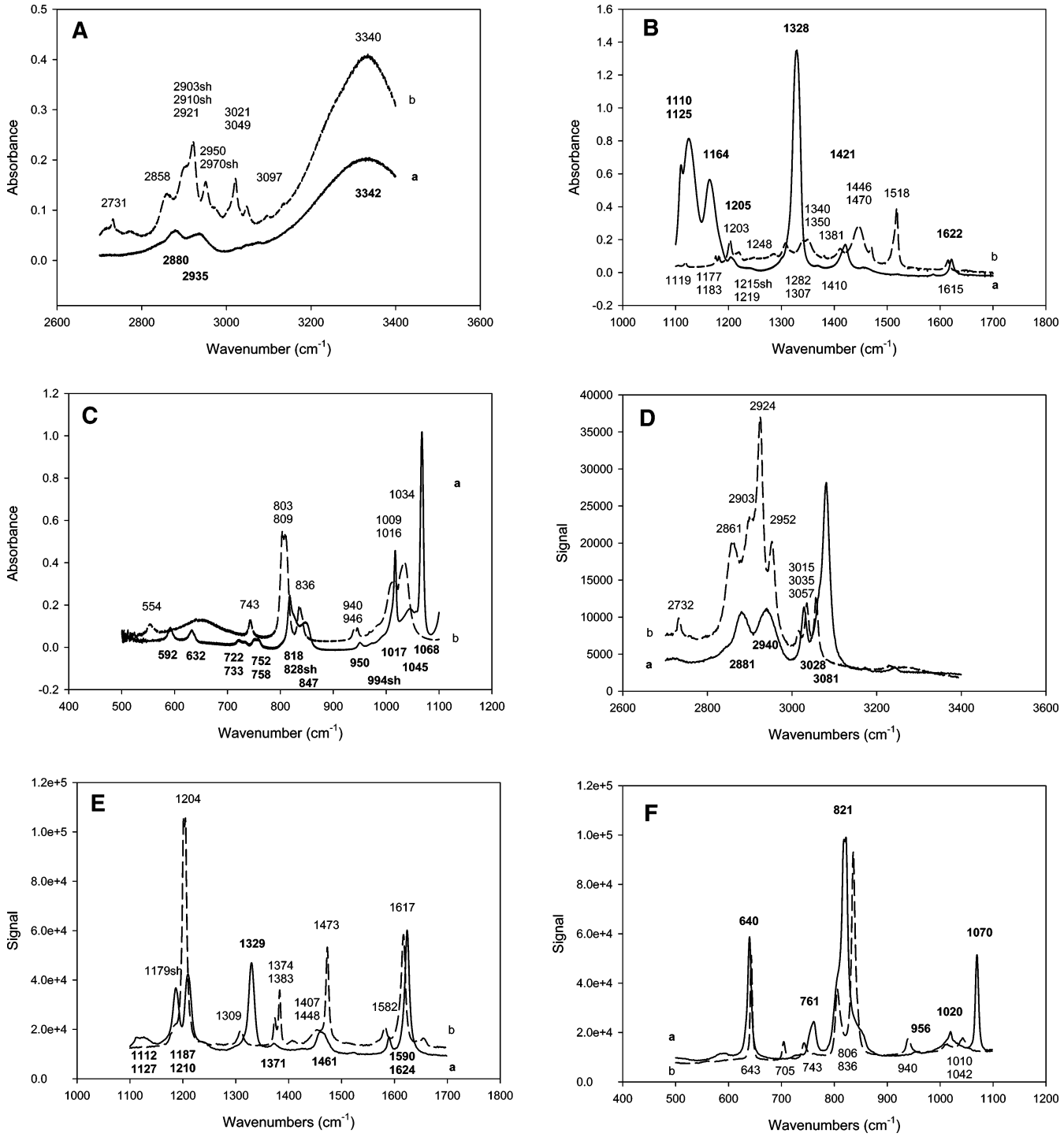

Figure 4. Spectra collected from (a) TFMBA and (b) MBA: FTIR spectra in the (A) high-, (B) medium-, and (C) low-frequency range, and Raman spectra in the (D) high-, (E) medium-, and (F) low-frequency range.

2.4. Fourier Transform Infrared Spectroscopy. FTIR spectra were collected with a Nicolet Magna-IR 550 FTIR spectrometer and processed with an OMNIC version 2.0 software package at 1 cm^{-1} resolution for 128 scans. Atmospheric water vapor was removed from the spectrometer housing by purging with dry nitrogen. The liquid samples were held between two NaCl plates, and the solid sample was mixed into a KBr pellet.

2.5. Computational Methods. TFMBA and other compounds were selected to make the ab initio calculations and spectral interpretations as simple as possible. All the compounds are simple benzyl alcohols; the only functional group to contain a C−F bond was a single trifluoromethyl group in TFMBA and TFMOBA, which was substituted by a corresponding methyl group in MBA and MOBA. The ab initio DFT calculations were performed with Gaussian03 B3LYP hybrid functions for exchange-correlation interactions with a 6-31++G** basis set (see Supporting Information for more details). The atomic numbering schemes for TFMBA (and MBA) and TFMOBA (and MOBA) are shown in Figure 1, panels a and b, respectively. Local symmetry coordinates are defined in Table 1. For the TFMOBA and MOBA samples, a water molecule was included in the calculation to account for intermolecular hydrogen bonding at the site of the oxygen atom inserted between the CF_3 or CH_3 group and the benzene ring.

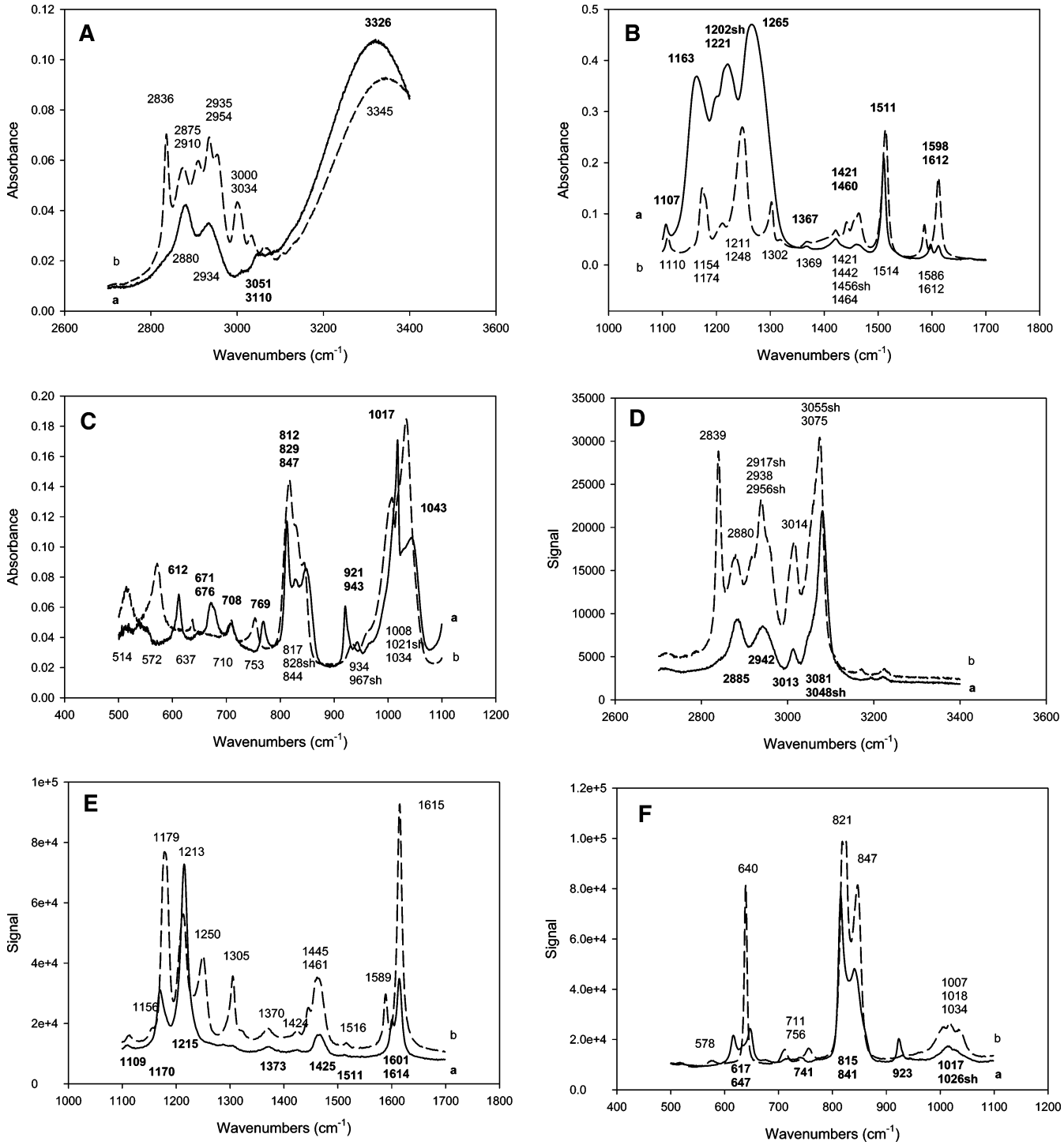

Figure 5. Spectra collected from (a) TFMOBA and (b) MOBA: FTIR spectra in the (A) high-, (B) medium-, and (C) low-frequency range, and Raman spectra in the (D) high-, (E) medium-, and (F) low-frequency range.

3. Results and Discussion

Chart 1 shows that all the four molecules have one common end CH_2OH group and a common aromatic group. The other ends of the molecules are different. They are CF_3, OCF_3, CH_3, and OCH_3 respectively. In the following discussion, we will first present SFG spectra collected in the C−H and C−F stretching regions, then we will discuss the FTIR and Raman spectra of these four compounds. After that, peak assignments will be reported according to ab initio calculations and FTIR and Raman spectra, which should provide an in-depth understanding of the SFG spectra.

3.1. SFG Spectra in the C−H Stretching Range. SFG spectra were collected from the liquid/air interfaces in the ssp polarization combination. Three ssp SFG spectra collected from TFMBA, TFMOBA, and MOBA in the C−H stretching range are shown in Figure 2. MBA is a crystalline solid; thus its SFG spectrum was not collected in air. Figure 2 shows that SFG signals were detected only from the MOBA/air interface, and no discernible C−H stretching signals could be detected from the TFMBA/air or TFMOBA/air interfaces. In addition, no SFG signals in the O−H stretching range were detected from TFMBA, TFMOBA, or MOBA in air (not shown). This clearly

TABLE 2: Peak Assignments for TFMBA[a]

$\nu_{obs,f}$ (cm^{-1})				
IR	Raman	$\nu_{calc,f}$	$\lvert d\mu/dQ\rvert^2$	potential energy and **IR intensity** distributions
S3342		3849	1.162	100(sOH); **86(sOH)**
		3233	0.019	95(s1415)
	S3081	3223	0.055	97(s910)
	W3063sh	3202	0.053	95(s1213)
	W3028	3174	0.276	98(s78)
W2935	M2940	3016	0.754	100(asCH_2); **91(asCH_2), 19(t3-9), −12(t1-6), 10(t2-7)**
W2880	M2881	2988	1.057	101(ssCH_2); **95(ssCH_2)**
W1622	VS1624	1667	0.568	135(b91112), 34(s79), 32(b7911), 30(s1214), 16(s911), 14(b679), 12(b111214), 10(s1112); **25(b367), 23(s911), 19(b121415), −15(b111213), 15(s1214), −14(b7910), 14(s1112), 13(sbCF_3), 12(b678), 12(s1116)**
	W1590	1627	0.030	47(s911), 33(b679), 31(b111214), 30(s1112), 25(s67)
		1557	0.002	78(b91112), 20(s911), 15(b678), 15(b111213), 13(b7910), 13(b121415), 12(s1112), 10(s67)
		1509	0.190	53(atHOCH), 38(sbOCH)
	M1461	1455	0.555	32(b7911), 24(sbOCH), 22(atHOCH), 18(s79), 11(s1214)
MW1421		1434	0.384	27(sbOCH), 26(atHOCH), 19(s1214), 13(s79), 12(bHOC), 11(b679); **47(bHOC), 23(sbOCH), 21(b7910), 20(b121415), 17(s1214), 10(as1CF_3)**
VW1368	VW1371	1360	0.181	51(s911), 35(s1112), 33(s67), 24(s79), 16(s1214)
VS1328	S1329	1327	8.699	89(b91112), 55(s1116), 53(b7911), 22(sbCF_3), 21(ssCF_3), 15(b111214); **50(sbCF_3), 28(ssCF_3), 11(s1116)**
	VW1302sh	1345	0.065	23(b678), 22(b111213), 20(b121415), 19(b7910)
		1257	0.000	84(abOCH)
	VW1237sh	1237	0.147	30(b91112), 24(s36), 15(b7911), 15(s67), 13(s1214), 11(sbOCH)
VW1205	S1210	1212	0.438	19(b678), 17(b7910), 14(b111213), 14(b121415)
	M1187	1182	1.668	58(bHOC), 18(b679), 17(b91112), 14(b7911), 14(b121415), 13(s36); **80(bHOC), 27(sCO), 11(b679)**
MS1164		1168	2.296	49(as1CF_3), 22(at2CF_3), 10(s79); **87(as1CF_3), 28(at2CF_3)**
S1125	VW1127	1126	2.809	42(as1CF_3), 20(b7911), 16(at2CF_3), 12(s1214); **70(as1CF_3), 21(at2CF_3)**
MS1110	VW1112	1117	6.581	96(as2CF_3), 48(at1CF_3), 18(ab2CF_3); **75(as2CF_3), 25(at1CF_3)**
S1068	M1070	1081	2.945	53(b91112), 25(ssCF_3), 24(s911), 20(sCO), 17(s1112), 14(sbCF_3); **54(sbCF_3), 41(ssCF_3), 27(sCO)**
MW1045		1073	1.451	71(sCO), 10(s911); **68(sCO), 18(as1CF_3), −10(b236)**
		1037	0.003	55(stHOCH), 24(abOCH), 12(t3-8)
M1017	W1020	1030	1.126	452(b7911), 207(b91112), 156(b679), 147(b111214); **41(sbCF_3), 33(ssCF_3), 16(b367), −15(b679)**
VW994sh		995	0.003	28(t9-13), 22(t11-15), 13(t9-14), 12(t3-8), 12(t6-11)
VW950	EW956	971	0.048	61(t7-12), 36(t6-11), 31(t6-10), 24(t3-8), 16(t9-14)
MW847	W849sh	862	0.111	47(t11-15), 37(t9-13), 14(t6-10), 13(t3-8), 10(t7-12)
W828sh		837	1.408	70(t7-12), 48(t3-8), 38(t9-14), 32(t6-10), 18(t11-15); **35(t3-8), −33(t7-12), 30(t6-10), 23(t11-15), 20(t6-11), 17(as2CF_3), 15(t2-7), −10(stCF_3)**
MW818	VS821	819	0.156	413(b91112), 122(b7911), 42(b111214), 20(s36), 10(ssCF_3)
VW758, VW752	MW761	736	0.181	96(b91112), 38(b7911), 33(ssCF_3), 23(sbCF_3), 14(b111214), 14(b679); **185(sbCF_3) −123(ssCF_3), 46(b236), 13(s1116), 12(bHOC), −11(b679), −10(s36)**
VW734, VW721	EW728	724	0.116	304(t7-12), 170(t6-11), 152(t9-14), 23(t9-13), 18(t6-10)
	S640	648	0.002	709(b7911), 228(b679), 217(b111214)
W632		620	0.112	156(b91112), 123(b679), 33(b111214), 26(b236), 20(sbCF_3); **120(sbCF_3), −25(b679), 18(bHOC), −17(ssCF_3), −17(as1CF_3), 13(at2CF_3), 11(b121415), 10(b91112), −10(b91116)**
W592	VW594	588	0.183	39(at1CF_3), 26(t6-11), 17(ab2CF_3)
		566	0.013	63(at2CF_3), 39(b7911), 14(as1CF_3), 12(ab1CF_3), 10(b111214)
		490	0.061	140(t7-12), 73(t9-14), 34(at1CF_3), 16(t9-13), 14(stHOCH)

[a] Abbreviations: sh = shoulder, E = extremely, V = very, W = weak, M = medium, and S = strong. Observed band intensities are described as EW, VW, MW, W, M, MS, S, or VS in increasing order. Such abbreviations have also been used in Tables 3−5.

demonstrates that for TFMBA and TFMOBA, which have fluorinated groups in the molecule, the end CH_2OH and the aromatic group either do not segregate to the surface or they are disordered or lie down on the surface. Since air is quite hydrophobic, and the fluorinated end groups in these two molecules are also very hydrophobic, the fluorinated end groups should segregate to the surface due to the favorable hydrophobic interactions. Therefore we believe the absence of C−H signals indicates that the CH_2OH and aromatic groups are not present on the TFMBA or TFMOBA surfaces.

A prominent peak at ~2830 cm^{-1} can be detected from the MOBA surface in air, which is due to the C−H symmetric stretching mode of the OCH_3 group.[35] SFG signals from C−H stretching modes of the aromatic group or the CH_2OH end group were not observed. Since the end OCH_3 group is more hydrophobic than the end CH_2OH group, it should segregate to the surface in preference to the CH_2OH group. We believe that the OCH_3 groups dominate the MOBA surface in air.

3.2. SFG Spectra in the C−F Stretching Range. As mentioned above, SFG signals for C−F stretching modes have been observed for CF_2, but SFG signals from CF_3 groups have not been reported yet. Here, we collected ssp SFG spectra from TFMBA, TFMOBA, and MOBA surfaces in air in the low-frequency range (1100−1700 cm^{-1}). No SFG signal was detected from either the TFMOBA or the MOBA surface, but a strong signal at ~1328 cm^{-1} was detected from the TFMBA/air interface (Figure 3). No sps signal was detected from any of the three surfaces in air.

It is reasonable that no strong SFG signal was detected from MOBA, because in this low-frequency range no strong stretching signals can be generated from the surface-dominating OCH_3 groups. We believe that the strong signal from the TFMBA surface must be related to the CF_3 end groups, because it is in the appropriate frequency range for CF_3 stretching signals. Unexpectedly, no such signals were detected at this range from the TFMOBA surface in air, in spite of the presence

TABLE 3: Peak Assignments for TFMOBA

ν_{obs} (cm^{-1})				
IR	Raman	ν_{calc}	$\lvert d\mu/dQ\rvert^2$	potential energy and **IR intensity** distributions
S3326		3850	1.110	100(sOH); **85(sOH)**
	S3081	3242	0.028	80(s1213), 20(s1415)
VW3059sh	W3062sh	3226	0.009	80(s1415), 20(s1213)
W3051	MW3048sh	3218	0.222	97(s910)
VW3010	W3013	3176	0.300	98(s78)
W2934	M2942	3013	0.822	100(asCH_2); **90(asCH_2), 21(t3-9), −12(t1-6)**
MW2880	M2885	2986	1.189	101(ssCH_2); **95(ssCH_2)**
W1612	MS1614	1662	0.049	105(b91112), 35(s79), 26(s1214), 25(b679), 23(s911), 18(b111214), 13(b7911)
W1598	MW1601	1641	0.271	120(b7911), 40(s1112), 36(s911), 28(s67), 25(b111214), 21(b679)
S1511	EW1511	1550	2.655	85(b91112), 25(s911), 18(b7910), 17(b111213), 12(b678), 12(s1112), 12(b121415), 10(s67); **48(s1116), 16(b7910), 14(b121415), 12(b111213)**
		1511	0.223	54(atHOCH), 36(sbOCH)
VW1460	MW1467, MW1461	1459	0.135	26(b7911), 20(s79), 19(s1214), 14(sbOCH), 14(b111213), 13(atHOCH)
W1421	EW1425	1436	0.290	39(sbOCH), 33(atHOCH), 14(bHOC), 12(s1214)
VW1367	VW1373	1361	0.871	35(s911), 33(s1112), 28(s67), 24(s79), 10(s1214)
		1350	0.417	26(b121415), 25(b678), 15(b111213), 13(s911), 12(b7910), 11(s1112)
VS1265		1264	24.731	74(s1617), 26(sbCF_3), 20(ssCF_3); **33(s1617), 24(sbCF_3), 17(s1116), 14(ssCF_3)**
		1255	0.001	84(abOCH)
S1221		1238	1.399	49(b91112), 20(s36), 19(b7911), 15(s1214), 12(b7910), 12(s67), 11(b111214); **43(as1CF_3), 21(at2CF_3), 19(bHOC), 16(s1116), 15(sbOCH), −10(b7910), −10(sCO)**
	VS1215	1220	0.942	61(b91112), 22(b7911), 20(b678), 19(s1116), 15(b121415), 12(s79), 11(b111214), 10(s1214); **93(s1116), 26(bHOC), −15(b678), 13(b7911), −11(b679), −11(b121415)**
MS1202sh		1215	2.171	68(b91112), 23(s911), 20(as1CF_3), 14(s1116), 12(b7911), 12(at2CF_3), 10(b7910), 10(b111214); **55(as1CF_3), 29(s1116), −23(bHOC), 21(at2CF_3), 10(sbCF_3)**
		1195	3.620	80(b91112), 52(as1CF_3), 34(b7911), 23(at2CF_3), 16(s1116), 12(s1617); **46(as1CF_3), 19(s1617), 11(at2CF_3)**
	M1170	1183	2.374	56(bHOC), 16(b121415), 13(b679), 13(s36), 11(b7911); **66(bHOC), 23(sCO), 11(b679)**
VS1163		1156	8.450	96(as2CF_3), 45(at1CF_3), 23(ab2CF_3); **65(as2CF_3), 25(at1CF_3)**
W1107	VW1109	1151	0.220	23(s1214), 17(b7910), 16(s79), 15(b7911), 13(b679), 13(b121415), 11(b678)
M1043		1073	1.394	93(sCO); **103(sCO), −25(b236), 25(b367)**
W1027sh	W1026sh	1038	0.000	58(stHOCH), 24(abOCH), 11(t3-8)
M1017	W1017	1036	0.386	405(b7911), 137(b679), 126(b111214), 120(b91112), 19(s911), 12(s1112), 11(b678), 10(b111213)
VW965sh		987	0.046	32(t6-11), 28(t3-8), 22(t7-12), 18(t6-10), 15(t11-15), 10(t9-13)
VW943		961	0.000	38(t7-12), 25(t9-14), 22(t11-15), 18(t6-10), 13(t9-13), 12(t6-11)
W921	W923	931	0.486	46(ssCF_3), 31(b679), 24(b7911), 21(b91112), 16(s911); **104(ssCF_3), 64(sbCF_3), −37(s1617), −23(s1116)**
M847	MS841	847	0.522	59(t3-8), 49(t6-10), 14(t7-12), 11(t9-13)
W829		831	0.925	53(t7-12), 52(t11-15), 39(t9-13), 35(t9-14); **47(t11-15), 46(t9-13), −25(t7-12), 22(t11-22), −17(t9-21), 12(t3-8), 11(t6-11)**
M812	S815	825	0.507	309(b91112), 75(b7911), 34(b111214), 17(ssCF_3), 13(s1116), 13(s36), 11(b91116)
W769		768	0.008	263(b91112), 113(b7911), 33(b111214), 16(s36), 12(b111617), 11(b679), 11(ab1CF_3)
VW708		688	0.011	401(t7-12), 212(t6-11), 193(t9-14), 16(t9-13), 14(t6-10)
W671		686	0.045	68(b7911), 51(b679), 33(sbCF_3), 14(ssCF_3), 12(b91116); **365(sbCF_3), −146(ssCF_3), −48(s1617), −43(bCO:H), −40(b111617), −34(s1116), 25(at2CF_3), 14(b91116), 13(ab1CF_3), 11(b679), −10(b111214)**
	MW647	638	0.017	696(b7911), 184(b111214), 161(b679), 11(b91112)
W612	W617	604	0.261	219(b91112), 140(b679), 69(b111214), 24(b236), 16(sbCF_3); **70(sbCF_3), 35(b236), −35(b679), 23(b91116), 17(bHOC), −14(as1CF3), 10(b111214)**
		600	0.031	60(at1CF_3), 34(ab2CF_3), 14(as2CF_3)

of a CF_3 group. The only difference between TFMBA and TFMOBA is that the CF_3 group in TFMBA is directly connected to the aromatic group, while in TFMOBA the CF_3 group is connected to an oxygen atom, and the oxygen atom is connected to the aromatic group. The presence or absence of the SFG peak at 1328 cm^{-1} must be related to the absence or presence of the oxygen atom in the molecule. We will confirm this assumption and present detailed interpretation of this observed phenomenon in the following analysis.

3.3. FTIR and Raman Spectra. The SFG transition hyperpolarizability is a product of the IR transition dipole moment and Raman polarizability.[16−32] Therefore, SFG spectra can be interpreted by understanding FTIR and Raman spectra. Normally, SFG detects only vibrational modes of ordered surface/interface functional groups with certain orientations that are both IR- and Raman-active. FTIR and Raman can probe many more vibrational modes, including modes of bulk functional groups or surface-disordered groups. Therefore, here we collected FTIR and Raman spectra of TFMBA, TFMOBA, and MOBA molecules. For comparison purposes, FTIR and Raman spectra for MBA have also been collected. We collected these FTIR and Raman spectra over a broad frequency range (500−3400 cm^{-1} for both FTIR and Raman spectra). Figure 4 shows the FTIR and Raman spectra collected from TFMBA and MBA, and Figure 5 displays the FTIR and Raman spectra from TFMOBA and MOBA. A strong peak at ∼1328 cm^{-1} has been observed in both the FTIR and Raman spectra of TFMBA; therefore it is natural to observe such a peak in the SFG spectrum of TFMBA. For the other three molecules, no strong signal was detected in the FTIR or Raman spectra at this position, and thus no SFG signal at 1328 cm^{-1} has been detected in these compounds. In the following, we will provide in-depth understanding of this vibrational mode. Figures 4 and 5 show that several peaks in the range of 1000−1700 have both strong FTIR and Raman signals, but none of them was detected by SFG, as shown in Figure 3. Therefore, to obtain further understanding of vibrational modes of these

TABLE 4: Peak Assignments for MBA

$\nu_{obs,f}$ (cm^{-1})				
IR	Raman	ν_{calc}	$\lvert d\mu/dQ\rvert^2$	potential energy and **IR intensity** distributions
M3340		3849	0.961	100(sOH); **86(sOH)**
VW3097		3222	0.064	98(s1415)
W3049	S3057	3181	0.538	80(s910), 19(s78)
	M3035	3168	0.450	97(s1213)
MW3021				2 × 1518ir = 3036
VW3013sh	MW3015	3158	0.388	81(s78), 19(s910)
VW2970	VW2974sh	3114	0.465	98(as1CH_3); **94(as1CH_3)**
		3084	0.435	101(as2CH_3); **97(as2CH_3)**
W2950	M2952	3008	0.934	100(asCH_2); **91(asCH_2), 19(t3-9), −11(t1-6)**
M2921	MS2924	3031	0.947	98(ssCH_3); **104(ssCH_3)**
M2910sh	W2910sh			2 × 1470ir = 2940 (2 × 1473R = 2946)
M2903sh	MW2902			2 × 1446ir = 2892 (2 × 1448R = 2896): weak Fermi resonance with unperturbed ssCH_2 around 2880
MW2858	MW2861	2982	1.340	101(ssCH_2); **95(ssCH_2)**
W2731	VW2733			2 × 1381 = 2762 or 1470 + 1307 = 2777
	VW1654			2 × 836 = 1672
W1615	VS1617	1666	0.006	133(b91112), 34(s79), 33(b7911), 29(s1214), 16(s911), 14(b679), 12(b111214), 10(s1112)
	M1582	1621	0.019	93(b7911), 40(s911), 33(b679), 31(b111214), 28(s1112), 26(s67)
S1518		1554	0.527	81(b91112), 23(s911), 14(b678), 14(b7910), 14(b111213), 13(s1112), 13(b121415), 11(s67); **32(b121415), 18(b367), 14(b678), 14(b111213), 12(b7910), 10(s1116), 10(s36)**
		1512	0.173	55(atHOCH), 36(sbOCH)
W1470	M1473	1500	0.329	57(at2CH_3), 10(ab1CH_3)
		1490	0.160	69(at1CH_3)
MS1446	W1448	1449	0.374	32(b7911), 29(sbOCH), 24(atHOCH), 14(s79), 10(s1214)
W1410	VW1407	1432	0.291	24(sbOCH), 21(s1214), 21(atHOCH), 15(s79), 11(b679), 11(bHOC)
VW1381	M1383	1419	0.006	102(sbCH_3)
	VW1374	1348	0.176	42(s911), 30(s1112), 29(s67), 23(s79), 12(s1214)
M1350				809 + 553 = 1362
W1340				803 + 553 = 1356
W1307	VW1309	1341	0.042	22(b678), 21(b121415), 18(s911), 17(b111213), 15(b7910), 11(s1112)
VW1282				2 × 644 = 1288
VW1248		1255	0.001	84(abOCH)
	VW1237	1238	0.095	128(b91112), 63(b7911), 23(b111214), 18(s36), 17(b679), 14(b7910), 13(s67)
VW1219		1230	0.060	105(b91112), 40(b7911), 36(s1116), 17(s1214), 14(s911), 13(s79), 12(b111214)
MW1203	VS1204	1210	0.119	20(b678), 17(b7910), 15(b111213), 13(b121415), 10(s79)
W1183, W1177	M1179	1181	2.041	56(bHOC), 14(b679), 14(b121415), 13(s36); **69(bHOC), 25(sCO), 13(b679)**
VW1119		1141	0.171	19(s1214), 18(s79), 15(b7910), 14(b121415), 13(b111213), 12(b679), 10(b678)
MS1034	W1042	1070	1.492	90(sCO); **99(sCO), −23(b236), 22(b367)**
		1062	0.075	92(ab2CH_3), 46(at1CH_3), 37(t7-12), 18(t9-14)
		1037	0.004	57(stHOCH), 24(abOCH), 11(t3-8)
M1016		1035	0.182	418(b7911), 142(b679), 133(b91112), 129(b111214), 17(s911), 11(b111213), 11(b678)
MW1009sh	VW1010	1006	0.148	86(ab1CH_3), 39(at2CH_3), 24(b7911), 14(s911), 11(s1112), 10(b111214)
VW984sh		983	0.006	27(t9-13), 25(t11-15), 14(t6-11), 10(t9-14), 10(t3-8)
VW946, VW940	VW940	952	0.002	37(t7-12), 31(t6-11), 29(t3-8), 26(t6-10)
		855	0.039	39(t9-13), 36(t11-15), 20(t3-8), 18(t6-10)
MW836	VS836	835	0.041	233(b91112), 56(b7911), 21(b679), 21(b111214), 19(s911), 14(s1116), 14(s1112), 13(s36)
MS809, MS803	M806	810	1.179	42(t3-8), 39(t6-10), 30(t7-12), 19(t11-15), 17(t9-14); **34(t3-8), 34(t6-10), 26(t11-15), −22(t7-12), 17(t9-13), 15(t2-7)**
W743	VW743	730	0.096	182(b91112), 70(b7911), 45(b679), 32(b111214), 21(s1116), 21(s36), 12(b236), 10(s911)
	VW705	699	0.004	346(t7-12), 209(t6-11), 165(t9-14), 11(t9-13), 10(t6-10)
M641	MS643	653	0.004	690(b7911), 244(b679), 212(b111214)
W554		544	0.241	432(b91112), 71(b111214), 65(b679), 45(b7911), 43(b236), 11(b91116)

four compounds, we assigned vibrational peaks in all frequency ranges in Figures 4 and 5 through ab initio calculation.

3.4. Peak Assignment for SFG Spectra. To ensure the reliability of our peak assignment by ab initio calculation, we analyzed many vibrational peaks in Figures 4 and 5. Tables 2−5 list experimental data as well as ab initio calculation results for TFMBA, TFMOBA, MBA, and MOBA, respectively. In Tables 2−5, observed FTIR and Raman peak centers, calculated vibrational frequency, calculated IR transition dipole moment, potential energy distribution, and IR intensity distribution are listed. Detailed analyses and interpretations of the various vibrational peaks and modes are presented in the Supporting Information. Here we will analyze the assignment for the observed SFG signals at 1328 cm^{-1} for TFMBA. As mentioned, the corresponding IR peak (VS1328ir) dominates the IR spectrum for this material (Figure 4), which is to be expected for the strong C−F dipole. A corresponding Raman peak (S1329R) has also been detected (Figure 4). According to the DFT results, this mode comprises mainly symmetric stretching and bending vibrations (ssCF_3, sbCF_3) coupled with adjacent stretching and bending modes (s1116, b91112) in the aromatic ring. The degree of coupling here between an aromatic ring and an adjacent functional group is substantial and may be attributed to the considerable electronegativity of the fluorines of the CF_3 group. Because sbCF_3 and ssCF_3 modes belong to the same irreducible representation, strong coupling between the sbCF_3 and ssCF_3 vibration can then be expected. In addition, the s1116 and b91112 vibrations (which belong to the same local symmetry species as the sbCF_3 and ssCF_3 vibrations) also interact with the CF_3 group. Therefore the detection of this peak in SFG is due to the strong coupling between the stretching/

TABLE 5: Peak Assignments for MOBA

ν_{obs} (cm^{-1})				
IR	Raman	ν_{calc}	$\lvert d\mu/dQ\rvert^2$	potential energy and **IR intensity** distributions
S3345		3849	0.994	100(sOH); **84(sOH)**
	S3075	3230	0.127	63(s1415), 37(s1213)
	W3055sh	3215	0.119	59(s1213), 34(s1415)
VW3034		3213	0.002	90(s910)
	W3014	3168	0.386	97(s78)
W3000				Fermi resonance of $ssCH_3$; 2 × VS1514ir = 3028
		3148	0.527	92($as1CH_3$)
MW2954	MW2953sh	3091	0.781	101($as2CH_3$)
		3024	1.318	93($ssCH_3$); **87(ssCH3), 15(s1617)**
MW2935	M2938	3007	0.932	100($asCH_2$); **89($asCH_2$), 21(t3-9), −11(t1-6)**
W2910	W2917			2 × MW1464ir (MS1462R) = 2928 (2922)
W2875	M2880	2982	1.403	101($ssCH_2$); **96($ssCH_2$)**
M2836	MS2839			strong Fermi resonance of an overtone of $sbCH_3$ (2 × W1442ir = 2884) with ssCH3 (2924R and 2921ir for 4-methyl benzylalcohol)
S1612	VS1615	1666	0.639	118(b91112), 38(s79), 25(s1214), 22(b679), 22(b7911), 19(s911), 16(b111214), 10(b678)
M1586	M1589	1630	0.945	96(b7911), 30(s1112), 26(s911), 22(s67), 20(b111214), 19(b679)
VS1514	VW1516	1552	3.208	96(b91112), 28(s911), 16(b7910), 15(b111213), 13(b678), 12(s67), 10(s1112), 10(b121415); **50(s1116), 13(s911), 12(b7910), 12(b121415)**
		1513	0.081	53(atHOCH), 34(sbOCH)
MW1464	MS1461	1512	0.818	62($at2CH_3$), 13($ab1CH_3$); **52($at2CH_3$), 23(s1116), 13($ab1CH_3$)**
		1494	0.194	79($at1CH_3$); **103($at1CH_3$), 24(t11-22), 16($ab2CH_3$), −16(t16-23)**
W1456sh		1459	0.431	24(b7911), 21(s79), 19(s1214), 17(sbOCH), 15(atHOCH), 11(b111213), 10(b111214)
W1442	W1445	1479	0.068	98($sbCH_3$)
W1421	VW1424	1435	0.354	36(sbOCH), 30(atHOCH), 14(s1214), 13(bHOC), 10(b679), 10(s79)
VW1369	VW1370	1364	0.557	36(s911), 35(s1112), 26(s67), 26(s79)
M1302	MW1305	1343	0.065	25(b121415), 23(b678), 18(b111213), 14(b7910), 12(s911)
VS1248	M1250	1267	5.773	132(b91112), 52(b7911), 51(s1116), 27(b111214), 17(s911), 12(s1214), 11(s1617), 10($ab1CH_3$); **78(s1116), 21(s1617), 14(b7911)**
		1254	0.001	84(abOCH)
W1211	1213M	1235	0.037	33(b91112), 23(s36), 19(b7911), 18(s67), 16(s1214), 11(sbOCH)
		1210	0.591	41(b91112), 18(b7910), 17(b7911), 16(b678), 16(b111213), 12(bHOC)
		1206	0.246	74($ab1CH_3$), 33($at2CH_3$), 23(b91112), 12(b7911)
M1174	S1179	1183	2.316	54(bHOC), 18(b121415), 13(b679), 13(s36); **60(bHOC), 22(sCO), 16(b679)**
VW1154	VW1156sh	1170	0.016	103($ab2CH_3$), 34($at1CH_3$)
W1110	VW1113	1146	0.242	23(b7911), 22(s1214), 18(b7910), 14(s79), 14(b121415), 10(b678)
S1034	W1034	1074	2.037	55(sCO), 42(b91112), 33(s1617); **52(sCO), 42(s1617), 17(b367), −16(b91116), −11(b236)**
W1021sh	MW1018	1060	1.021	48(s1617), 39(sCO), 16(b91112), 11(s911**);** **82(s1617), 42(sCO), 19(b91116), −14(b236), −12(s1116)**
		1038	0.000	60(stHOCH), 24(abOCH), 10(t3-8)
M1008	MW1007	1029	0.106	410(b7911), 155(b679), 129(b111214), 116(b91112), 17(s911), 12(b111213), 11(s1112), 10(b678)
VW967sh		972	0.015	30(t3-8), 28(t6-11), 19(t11-15), 16(t7-12), 13(t6-10), 10(t9-13)
VW934	VW934	944	0.001	34(t7-12), 24(t11-15), 19(t9-14), 16(t6-10), 14(t6-11), 14(t3-8), 10(t9-13)
MW844	M847	838	0.702	54(t6-10), 53(t3-8), 37(t7-12), 16(t9-14)
W828		822	0.972	58(t7-12), 47(t11-15), 46(t9-13), 37(t9-14); **48(t9-13), 42(t11-15), 16(t6-11)**
M817	VS821	837	0.363	277(b91112), 62(b7911), 29(b111214), 19(b679), 16(s911), 14(s1112), 14(s36), 12(s1116)
W753	VW756	735	0.175	150(b91112), 67(b7911), 37(b679), 28(b111214), 18(s1116), 18(s36), 12(b236)
VW710	VW711	689	0.028	384(t7-12), 200(t6-11), 184(t9-14), 18(t9-13), 16(t6-10)
VW637	M640	647	0.008	697(b7911), 280(b679), 201(b111214)
MW572	VW578	548	0.946	391(b91112), 180(b7911), 32(b679), 30(b236), 25(b111617), 15(b111214)
W514	VW517	518	0.379	128(t7-12), 48(t9-14), 27(t9-13), 14(stHOCH), 13(t7-16)

bending modes of the CF_3 groups and vibrational modes of other groups in the molecule.

Other modes for TFMBA related to the $sbCF_3$ and $ssCF_3$ vibrations are identified as the observed bands S1068ir (M1070R), M1017ir (W1020R), VW758ir (MW761R), and W632ir. A strong SFG peak corresponding to the band S1068ir (M1070R) might be expected, but at this frequency our input IR energy was very low and this peak was not detected in the SFG spectrum. The strong infrared bands MS1164, S1125, and MS1110 for TFMBA closely match the calculated modes related to asymmetric stretching and bending vibrations of the CF_3 group. The weakness of the corresponding Raman intensities is consistent with the absence of any corresponding SFG peaks. This explains why only one peak at 1328 cm^{-1} was observed in the SFG spectrum of TFMBA.

The important coupling effect observed in TFMBA is more or less removed when an oxygen atom is inserted between the aromatic ring and the trifluoromethyl group in TFMOBA. Although the CF_3 peak is still dominant in the IR spectrum for this material (VS1265ir, Figure 5), the oxygen has reduced the frequency and changed the coupling behavior of the CF_3 group (ssCF3 and sbCF3 modes are now coupled with s1617 and s1116, not the aromatic ring). Although this peak should have been within our SFG range, no corresponding Raman peak was found (Figure 5), and no SFG peak was detected. Therefore we believe that the strong coupling in TFMBA is important to ensure the observation of the SFG CF_3 signal. Such an SFG peak was not observed from TFMOBA is because of the lack of such coupling. Similar to TFMBA, the other IR bands of TFMOBA involving CF_3 either lack corresponding Raman activity or lie below our current SFG range (see more details in Supporting Information).

4. Conclusion

In the above experiments, we have for the first time successfully used SFG to detect ordered CF_3 groups at an

interface. The strong correlations between the SFG, IR, Raman, and DFT data allow reliable peak assignments to be made for all the available spectral information. The considerable coupling ability of the CF_3 group has been demonstrated by our investigations of these small model compounds. We have also shown that the vibrational coupling and SFG activity of the CF_3 group can be significantly affected by the insertion of an oxygen atom between the CF_3 group and the rest of the molecule. The interfacial behavior of the extremely hydrophobic CF_3 group is important in a variety of materials, including liquids, surfactants, and polymers. In the case of highly fluorinated polymers, terminal CF_3 groups are commonly used to make such materials amorphous, and the interfacial distribution of these groups governs the interfacial properties of the material. This work has demonstrated the feasibility of detecting CF_3 groups at a surface and should contribute to a basis for further interfacial studies on more complicated fluorinated materials. An orientation analysis of fluorinated functional groups will be performed in the future. Our most recent studies indicate that it is feasible to detect C−F stretching signals from self-assembled monolayers with fluorinated end groups, perhaps due to the very ordered structure of the C−F groups. More details regarding such research will be reported in the future.

Acknowledgment. This work was supported by the Office of Naval Research (N00014-02-1-0832) and National Science Foundation (CHE-0449469). We greatly appreciate the help in Raman experiments from Mr. Adam L. Grzesiak and Professor Adam J. Matzger at the Department of Chemistry of the University of Michigan.

Supporting Information Available: Detailed discussion regarding the ab initio method and peak assignments. This material is available free of charge via the Internet at http://pubs.acs.org.

References and Notes

(1) Smart, B. E. In *Organofluorine Chemistry: Principles and Commercial Applications*; Banks, R. E., Smart, B. E., Tatlow, J. T., Eds.; Plenum Press: New York, 1994.
(2) Callow, M. E.; Fletcher, R. L. *Int. Biodeterior. Biodegrad.* **1994**, *34*, 333−348.
(3) Mera, A. E.; Goodwin, M.; Pike, J. K.; Wynne, K. J. *Polymer* **1999**, *40*, 419−427.
(4) Brady, R. F.; Aronson, C. L. *Biofouling* **2003**, *19*, 59−62.
(5) Youngblood, J. P.; Andruzzi, L.; Ober, C. K.; Hexemer, A.; Kramer, E. J.; Callow, J. A.; Finlay, J. A.; Callow, M. E. *Biofouling* **2003**, *19*, 91−98.
(6) Bernett, M. K.; Ravner, H. *J. Adhes.* **1978**, *9*, 157−166.
(7) Park, I. J.; Lee, S.-B.; Choi, C. K.; Kim, K.-J. *J. Colloid Interface Sci.* **1996**, *181*, 284−288.
(8) Krupers, M.; Slangen, P. J. Möller, M. *Macromolecules* **1998**, *31*, 2552−2558.
(9) Tirelli, N.; Ahumada, O.; Suter, U. W.; Menzel, H.; Castelvetro, V. *Macromol. Chem. Phys.* **1998**, *199*, 2425−2431.
(10) Castelvetro, V.; Ciardelli, F.; Francini, G.; Baglioni, P. *Macromol. Mater. Eng.* **2000**, *278*, 6−16.
(11) Böker, A.; Reihs, K.; Wang, J.; Stadler, R.; Ober, C. *Macromolecules* **2000**, *33*, 1310−1320.
(12) Castelvetro, V.; Aglietto, M.; Ciardelli, F.; Chiantore, O.; Lazzari, M.; Toniolo, L. *J. Coat. Technol.* **2002**, *928*, 57−66.
(13) Imae, T. *Curr. Opin. Colloid Interface Sci.* **2003**, *8*, 307−314.
(14) Woodruff, D.; Delchar, T. *Modern Techniques of Surface Science*; Cambridge University Press: Cambridge, U.K., 1986.
(15) Somorjai, G. A. *Introduction to Surface Chemistry and Catalysis*; Wiley: New York, 1994.
(16) Shen, Y. R. *The Principles of Nonlinear Optics*; Wiley: New York, 1984.
(17) Zhuang, X.; Miranda, P. B.; Kim, D.; Shen, Y. R. *Phys. Rev. B* **1999**, *59*, 12632−12640.
(18) Bain, C. D. *J. Chem. Soc., Faraday Trans.* **1995**, *91*, 1281−1296.
(19) Eisenthal, K. B. *Chem. Rev.* **1996**, *96*, 1343−1360.
(20) Scatena, L. F.; Brown, M. G.; Richmond, G. L. *Science* **2001**, *292*, 908−912.
(21) Gautam, K. S.; Schwab, A. D.; Dhinojwala, A.; Zhang, D.; Dougai, S. M.; Yeganeh, M. S. *Phys. Rev. Lett.* **2000**, *85*, 3854−3857.
(22) Chen, Z.; Shen, Y. R.; Somorjai, G. A. *Annu. Rev. Phys. Chem.* **2002**, *53*, 437−465.
(23) Wang, J.; Chen, C. Y.; Buck, S. M.; Chen, Z. *J. Phys. Chem. B* **2001**, *105*, 12118−12125.
(24) Wang, J.; Paszti, Z.; Even, E. A.; Chen, Z. *J. Am. Chem. Soc.* **2002**, *124*, 7016−7023.
(25) Briggman, K. A.; Stephenson, J. C.; Wallace, W. E.; Richter, L. J. *J. Phys. Chem. B* **2001**, *105*, 2785−2791.
(26) Bordenyuk, A. N.; Jayathilake, H.; Benderskii, A. V. *J. Phys. Chem. B* **2005**, *109*, 15941−15949.
(27) Ma, G.; Liu, D. F.; Allen, H. C. *Langmuir* **2004**, *20*, 11620−11629.
(28) Fitchett, B. A.; Conboy, J. C. *J. Phys. Chem. B* **2004**, *108*, 20255−20262.
(29) Ye, S.; Morita, S.; Li, G. F.; Noda, H.; Tanaka, M.; Uosaki, K.; Osawa, M. *Macromolecules* **2003**, *36*, 5694−5703.
(30) Kweskin, S. J.; Komvopoulos, K.; Somorjai, G. A. *Langmuir* **2005**, *21*, 3647−3652.
(31) Chou, K. C.; Kim, J.; Baldelli, S.; Somorjai, G. A. *J. Electroanal. Chem.* **2003**, *554*, 253−263.
(32) Rivera-Rubero, S.; Baldelli, S. *J. Phys. Chem. B* **2004**, *108*, 15133−15140.
(33) Ji, N.; Ostroverkhov, V.; Lagugné-Labarthet, F.; Shen, Y.-R. *J. Am. Chem. Soc.* **2003**, *125*, 14218−14219.
(34) Genzer, J.; Sivaniah, E.; Kramer, E. J.; Wang, J.; Körner, H.; Xiang, M.; Char, K.; Ober, C. K.; DeKoven, B. M.; Bubeck, R. A.; Chaudhury, M. J.; Sambasivan, S.; Fischer, D. A. *Macromolecules* **2000**, *33*, 1882−1887.
(35) Chen, Z.; Ward, R.; Tian, Y.; Baldelli, S.; Opdahl, A.; Shen, Y. R.; Somorjai, G. A. *J. Am. Chem. Soc.* **2000**, *122*, 10615−10620.